Journal of Catalysis 257 (2008) 152–162

Contents lists available at ScienceDirect

Journal of Catalysis

www.elsevier.com/locate/jcat

JOURNAL OF CATALYSIS

Carbon-templated hexaaluminates with enhanced surface area and catalytic performance

Marta Santiago [a], Johan C. Groen [b], Javier Pérez-Ramírez [a,c,*]

[a] Institute of Chemical Research of Catalonia (ICIQ), Avinguda Països Catalans 16, 43007 Tarragona, Spain
[b] DelftChemTech, Delft University of Technology, Julianalaan 136, 2628 BL, Delft, The Netherlands
[c] Catalan Institution for Research and Advanced Studies (ICREA), Passeig Lluís Companys 23, 08010 Barcelona, Spain

ARTICLE INFO

Article history:
Received 23 November 2007
Revised 2 March 2008
Accepted 19 April 2008
Available online 27 May 2008

Keywords:
High-temperature catalysis
Mixed oxides
Hexaaluminate
Template synthesis
Carbon
Porosity
N_2O decomposition

ABSTRACT

Carbon templating was used to synthesize high-surface area $LaFeAl_{11}O_{19}$ hexaaluminates leading to improved catalytic performance. The oxide precursor–template composites were prepared by impregnation, complexation with citric acid, and coprecipitation routes varying the amounts of acetylene black incorporated. Calcination in static air at 1473 K led to single-phased hexaaluminates. The samples were characterized at different stages of the synthetic protocol by ICP–OES, in situ and ex situ XRD, TEM, N_2 adsorption, He pycnometry, TGA, H_2-TPR, and XPS. The templating effect of carbon originates fine oxide particles. Consequently, the specific surface area of the non-templated hexaaluminates (1–11 $m^2\,g^{-1}$ depending on the preparation method) increased up to a factor of 25 upon incorporation of carbon in the synthesis. The stabilization of small particles occurs despite the temperature difference between the elimination of carbon (973 K) and the attainment of the hexaaluminate phase above 1373 K. The morphology of the oxide obtained upon carbon removal determines the textural properties of the hexaaluminate particles. Our results demonstrate that the confined space synthesis is not exclusively responsible for small oxide particles. The stabilization of small crystallites on the carbon surface in the composite and breakage of the oxide layer caused by template combustion are key aspects for attaining finely dispersed particles when the carbon is macroporous. The enhanced catalytic activity and time-on-stream stability of the templated hexaaluminates was demonstrated in the direct N_2O decomposition using model and simulated feed mixtures. In this application, a quasi-linear relation between the reaction rate and the specific surface area of the samples was obtained. Characterization by H_2-TRP and XPS indicated that the nature of iron in $LaFeAl_{11}O_{19}$ was not altered by carbon incorporation in the synthesis.

1. Introduction

Suitable catalysts for high-temperature applications should accomplish defined targets associated with activity and selectivity. However, only those materials additionally exhibiting extraordinary chemical and mechanical stability are ultimately implemented in industry. Metal-substituted hexaaluminates are attractive catalysts and catalyst supports for high-temperature applications, including natural gas combustion in power turbines [1–7], (partial) oxidation of hydrocarbons [8,9], CO_2-reforming of methane [10], and process-gas N_2O decomposition [11]. These materials exhibit stable phase composition up to 1873 K and remarkable resistance to sintering and thermal shock. These unique properties are associated with their structure, consisting of alternate stacking along the *c*-axis of γ-Al_2O_3 spinel blocks and mirror planes in which large alkaline (K^+), alkaline-earth (Ba^{2+}, Ca^{2+}, Sr^{2+}), or rare-earth (La^{3+}) cations are located [12]. Substitution of transition metal ions in Al^{3+} positions of the spinel blocks creates redox active centers in the structure with minimal effect on the sintering resistance of the material [1,3].

Hexaaluminate precursors are typically prepared by sol–gel synthesis using metal alkoxides or organometallic compounds [1,2,7,9] or coprecipitation of metal nitrate solutions with ammonium carbonate [5,6,11,13]. Calcination of the material above 1473 K results in single-phased metal-substituted hexaaluminates with specific surface areas in the typical range of 5–15 $m^2\,g^{-1}$ [14]. Increasing the surface area of hexaaluminates by novel or modified synthesis routes is of interest for prospective catalytic use. In the high-temperature regime, mass transfer usually plays an important role in the overall process and materials with large surface-to-volume ratios are advantageous. Zarur and Ying [15] introduced a reverse microemulsion-mediated sol–gel method to synthesize Ba-hexaaluminate nanoparticles with surface areas ranging from 40 to 160 $m^2\,g^{-1}$. However, this route is not amenable to industrial implementation due to economic, safety, and scalability con-

---

[*] Corresponding author at: Institute of Chemical Research of Catalonia (ICIQ), Avinguda Països Catalans 16, 43007 Tarragona, Spain. Fax: +34 977 920 224.
E-mail address: jperez@iciq.es (J. Pérez-Ramírez).

0021-9517/$ – see front matter
doi:10.1016/j.jcat.2008.04.017

straints. Metal alkoxides are harmful and expensive and their hydrolysis should be practiced under extremely controlled conditions (moisture and oxygen-free environment). Besides, relatively sophisticated freeze and supercritical drying techniques are necessary for nanoparticle recovery. Alluding to these limitations, Teng et al. [16] developed a reverse microemulsion route using inorganic salts and drying in supercritical ethanol, obtaining $BaMnAl_{11}O_{19}$ with 70 $m^2\,g^{-1}$.

Alternatively, templating approaches can be used to synthesize high-surface area materials with control over their structural and textural properties on length scales between nanometers and micrometers [17–19]. The concept of templating was introduced in the zeolite field and was extended to ordered mesoporous materials, where periodic pore systems are created by occlusion of molecular or supramolecular units in the resulting solid (referred to as ‘endotemplating’). A more recent approach is ‘exotemplating’ also termed ‘hard templating,’ ‘confined space synthesis,’ or ‘compartment solidification’ [17]. Exotemplates are extended porous structures providing the space where a divided solid can form. Carbon is the ideal exotemplate attending to its easy removal by combustion, versatile porous characteristics, and relatively low cost. Carbon templating has been applied to synthesize mesoporous zeolite crystals and nanocrystalline zeolites [20,21] as well as high-surface area oxides [22]. In the latter group, single metal oxides (e.g., MgO, Fe_2O_3, Cr_2O_3, TiO_2), spinels (e.g., $CoCr_2O_4$, $NiAl_2O_4$), and perovskites (e.g., $LaFeO_3$) with 4–20 times higher surface area than the non-templated counterparts have been obtained. However, most of these studies merely report increased surface area, and only exceptionally evaluate the effect of the created porosity on the catalytic performance [23].

The typical preparation of oxides by templating involves the impregnation of carbon with concentrated solutions of the metal cations followed by drying and thermal treatment [17,22]. To the best of our knowledge, other strategies to prepare the oxide precursor–carbon composites have not been widely explored. In addition, it is not straightforward to predict the effectiveness of carbon templating for synthesizing oxides requiring extremely high calcination temperatures, such as hexaaluminates. Work with oxides was restricted to perovskites requiring calcination temperatures up to 1073 K [22]. However, the radically different temperature between the combustion of carbon (typically 973 K) and the hexaaluminate formation (typically 1473 K) could lead to severe sintering of the intermediate oxidic phase once the carbon is removed, probably abrogating the template effect for achieving enhanced surface area and ultimately improved catalytic activity.

Herein we demonstrate the carbon templating route to prepare single-phased $LaFeAl_{11}O_{19}$ hexaaluminates (magnetoplumbite structure) with significantly higher surface area than the non-templated counterparts. Different methods to prepare the precursors have been practiced, incorporating variable carbon amounts. The materials were characterized by ICP–OES, in situ and ex situ XRD, TEM, N_2 adsorption, He pycnometry, TGA, H_2-TPR, and XPS. Based on these analyses, aspects of the templating mechanism are discussed. The templated hexaaluminates possess clear benefits in terms of catalytic performance compared to the carbon-free hexaaluminates, as illustrated by their application in direct N_2O decomposition using model and simulated mixtures. In our previous study [11], Fe-substituted hexaaluminates proved suitable catalysts for process-gas N_2O abatement in ammonia burners of nitric acid and caprolactam production. For this high-temperature application (1073–1173 K, wet oxidizing conditions), materials combining high catalytic activity and excellent chemical stability are required [24].

2. Experimental

2.1. Catalyst preparation

Hexaaluminates with the formula $LaFeAl_{11}O_{19}$ were obtained by calcination of differently prepared precursors. As starting point, an aqueous solution of the corresponding metal nitrates, i.e. $La(NO_3)_3{\cdot}6H_2O$, $Fe(NO_3)_3{\cdot}9H_2O$, and $Al(NO_3)_3{\cdot}9H_2O$ (Aldrich, purity $>98\%$), with 0.1 M La, 0.1 M Fe, and 1.1 M Al was prepared. Carbon black (acetylene, 50% compressed) from Alfa Aesar (product code 39724) was incorporated in the synthesis as the template. The carbon has a nominal surface area of 80 $m^2\,g^{-1}$. Previous to use, the as-received sample was dried at 378 K for 24 h. The carbon content given in the below recipes and in the code of the samples along the manuscript is expressed as weight percent with respect to the total weight of carbon and metal nitrates.

2.1.1. Impregnation

The precursor–template composite was prepared by a conventional impregnation method described elsewhere [22]. A fixed amount of carbon (40 wt% based on the total weight of carbon and metal nitrates) was impregnated with the aqueous solution of metal cations and mixed well with a spatula. This led to the formation of crumbly solid particles, which were dried at 363 K for 12 h and then calcined in static air at 1473 K for 1 h using a ramp of 5 $K\,min^{-1}$. The non-templated hexaaluminate counterpart was prepared using a solid-state route, i.e. mechanically mixing appropriate amounts of the metal nitrate salts followed by calcination according to the above program.

2.1.2. Complexation

A soft-chemical route equivalent to that described in [25] was carried out by mixing the solution of metal nitrates with citric acid at room temperature using a molar ratio of total cations to the complexant of 3 until a clear solution was obtained. Nominal carbon contents in the range 5–50 wt% were added to the resulting solution. Subsequently, the temperature of the resulting slurry was increased from 298 K to 433 K in static air using a heating rate of 0.7 $K\,min^{-1}$ and held for 12 h. The dried composite was crushed in an agate mortar followed by thermal treatment according to the program: heating from 433 K to 733 K at 5 $K\,min^{-1}$ and kept isothermal for 5 h, and finally heating to 1473 K at 5 $K\,min^{-1}$ for 1 h. The corresponding non-templated sample was prepared according to the same procedure without adding carbon to the solution of metal nitrates and citric acid.

2.1.3. Coprecipitation

A certain amount of carbon (nominal content of 25 and 50 wt%) was first impregnated by the solution of metal nitrates. Subsequently, an aqueous solution of 2 M $(NH_4)_2CO_3$ was added drop-wise under mechanical stirring (500 rpm) until pH 8.0 was reached. The slurry was aged at 333 K for 1 h, filtered, washed with deionized water, dried at 378 K for 12 h, and calcined in static air at 1473 K for 1 h using a heating rate of 5 $K\,min^{-1}$. The non-templated sample was prepared using the same coprecipitation method without the carbon impregnation step.

2.2. Catalyst characterization

The chemical composition was determined by Inductive Coupled Plasma–Optical Emission Spectroscopy (ICP–OES) (Perkin–Elmer Optima 3200RL (radial)). Prior to the analysis, the solids were treated using an alkaline fusion method with NaOH and Na_2O_2, followed by dilution with HCl.

Ex situ powder X-ray diffraction (XRD) patterns were acquired in a Bruker AXS D8 Advance diffractometer equipped with a Cu tube, a Ge(111) incident beam monochromator ($\lambda = 0.1541$ nm), and a Vantec-1 PSD. Data were collected in the 2θ range 10–70° with an angular step size of 0.02° and a counting time of 4 s per step.

In situ XRD during thermal decomposition of the precursors in air flow (100 ml STP min^{-1}) was studied in a Bruker AXS D5005 diffractometer equipped with a Bruker AXS MRI high-temperature chamber and a diffracted beam graphite monochromator using Cu$K\alpha$ radiation. A thin layer of sample (ca. 30 mg) was mounted on the Pt_{90}–Rh_{10} heater strip inside the chamber by placing a few droplets of a suspension of finely ground sample in ethanol on the strip followed by drying under ambient conditions. Data were collected in the 2θ range 10–70° with an angular step size of 0.05° and a counting time of 0.5 s per step. Patterns were recorded at intervals of 50 K in the range 323–1673 K after 2 min equilibration at each temperature. The heating rate was 60 $\text{K}\,\text{min}^{-1}$. The sample was directly heated by the heater strip, whose temperature can be controlled within 2 K.

Transmission Electron Microscopy (TEM) was carried out in a JEOL JEM-1011 microscope operated at 100 kV and equipped with a SIS Megaview III CCD camera. A few droplets of the sample suspended in ethanol were placed on a carbon-coated copper grid followed by evaporation at ambient conditions.

The skeleton density of selected solids was measured by helium pycnometry at 295 K in a Quantachrome Pentapycnometer. Prior to the measurement, the sample was dried at 393 K for 12 h.

Nitrogen adsorption–desorption isotherms at 77 K were measured on a Quantachrome Autosorb 6B analyzer. Before analysis, the samples were degassed in vacuum at 393 K for 16 h. The BET method [26] was applied to calculate the total surface area and the t-plot method [27] was used to discriminate between micro- and mesoporosity. The BJH model [28] applied to the adsorption branch of the isotherm provides information on the mesopore size distribution.

Thermal analysis was carried out in a Mettler Toledo TGA/SDTA 851e microbalance equipped with a 34-positions sample carrousel. The solid (3 mg) was placed in 70 μl-alumina crucibles without dilution. Analyses were performed in dry air flow (50 cm^3 STP min^{-1}), ramping the temperature from 298 to 1173 K with a heating rate of 5 $\text{K}\,\text{min}^{-1}$.

Temperature-programmed reduction with hydrogen (H_2-TPR) was carried out in a Thermo TPDRO 1100 system equipped with a thermal conductivity detector (TCD). The catalyst sample (150 mg) was loaded in the quartz micro-reactor (11 mm i.d.), pretreated in N_2 (20 ml STP min^{-1}) at 673 K for 1 h, and cooled to 323 K in the same atmosphere. The analysis was done in a high-purity mixture of 5 vol% H_2 in N_2 (20 ml STP min^{-1}), ramping the temperature from 323 to 1373 K at 10 $\text{K}\,\text{min}^{-1}$.

X-ray photoelectron spectroscopy (XPS) measurements were obtained using a PHI 5500 Multitechnique System from Physical Electronics equipped with monochromatic Al$K\alpha$ radiation at 1486.6 eV as the X-ray source, a nine-channeltron detection system, and a hemispheric electron analyzer operating at a constant pass energy of 23 eV and a resolution energy of 0.1 eV. The measurements were carried out in a UHV chamber, where the pressure was maintained between 5×10^{-9} and 2×10^{-8} Torr. The binding energies were referenced to the C 1s line at 284.8 eV.

2.3. Activity tests

Direct N_2O decomposition was studied in a quartz fixed-bed reactor (10 mm i.d.) using 200 mg of sample (sieve fraction 200–300 μm), a total pressure of 1 bar, and a weight-hourly space velocity (WHSV) of 60,000 $\text{ml}\,\text{g}^{-1}\,\text{h}^{-1}$. Isothermal tests were conducted in the range 573–1123 K, typically using a model mixture containing 1.5 mbar N_2O in He. Selected catalysts were additionally tested at 923 K in a feed mixture containing 1.5 mbar N_2O, 10 mbar NO, 100 mbar O_2, 100 mbar H_2O in He, i.e. simulating the gas composition at the outlet of the Pt–Rh gauzes in ammonia burners, where these catalytic systems can be potentially used [11]. Generally, 30 min after a change of conditions, the conversion levels were constant and considered as steady state. Prior to the tests, the catalysts were pretreated at 673 K in the feed mixture for 1 h. The reactant and product gases were analyzed by gas chromatography (SRA Instruments Micro-GC 3000) equipped with HP-PlotQ and HP-Plot MoleSieve columns and a TCD detector.

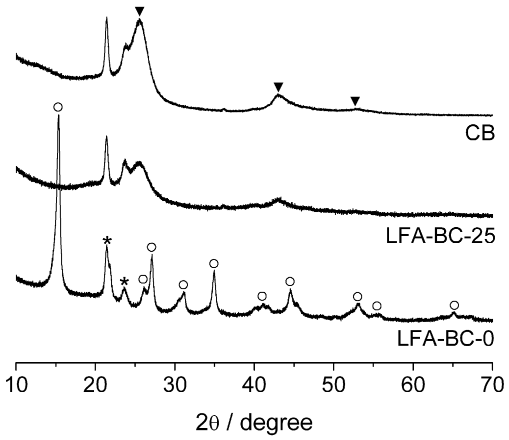

Fig. 1. Ex situ X-ray diffraction patterns of the hexaaluminate precursors prepared by coprecipitation in the absence (LFA-BC-0) or presence (LFA-BC-25) of carbon. The pattern of carbon (CB) is included for comparative purposes. Phases: (○) AACH, JCPDS 42-250; (▼) carbon, JCPDS 26-1080. The reflections marked by asterisk are due to the sample holder.

3. Results and discussion

The sample codes along the manuscript contain the initials of the metals in the hexaaluminate (LFA for La, Fe, and Al), the synthesis method (IM: impregnation, CA: complexation with citric acid, and BC: batch coprecipitation), and the nominal carbon content in the composite. For example, LFA-BC-0 and LFA-BC-25 denote the samples prepared by batch coprecipitation without carbon or with 25 wt% carbon, respectively.

3.1. Precursors

The precursors prepared with and without template were characterized by XRD (crystalline structure), TEM (morphology), N_2 adsorption–desorption at 77 K (porosity), and He pycnometry (density). Specifically, we elaborate here on the precursor and precursor–carbon composite synthesized by coprecipitation. The sample prepared in the absence of carbon (LFA-BC-0) presents characteristic reflections of ammonium aluminum carbonate hydroxide (AACH, $NH_4Al(OH)_2CO_3$) as the only crystalline phase (Fig. 1). As shown by transmission electron microscopy, the specimen consists of small irregular particles having a size distribution in the range 5–15 nm (Fig. 2, middle). The nitrogen isotherm of LFA-BC-0 (Fig. 3, open circles) evidences high uptake at $p/p_0 < 0.1$, indicative of a mostly microporous solid. As shown in Table 1, application of the t-plot method resulted in a micropore volume of 0.10 $\text{cm}^3\,\text{g}^{-1}$ and a mesopore surface area of 80 $\text{m}^2\,\text{g}^{-1}$, while the BET method estimated a much higher surface area (307 $\text{m}^2\,\text{g}^{-1}$) due to the microporosity.

Strikingly, none of the AACH diffraction lines in the XRD pattern of LFA-BC-0 were present in the LFA-BC-25 composite. The latter

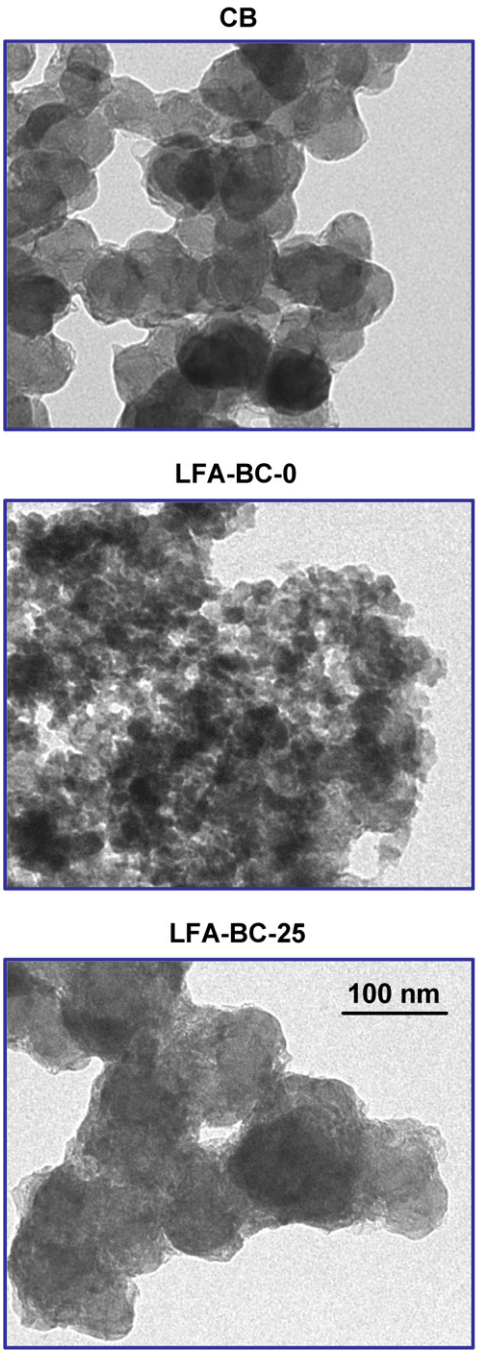

Fig. 2. Transmission electron micrographs of carbon (CB), precursor (LFA-BC-0), and precursor–carbon composite (LFA-BC-25). The scale applies to all the micrographs.

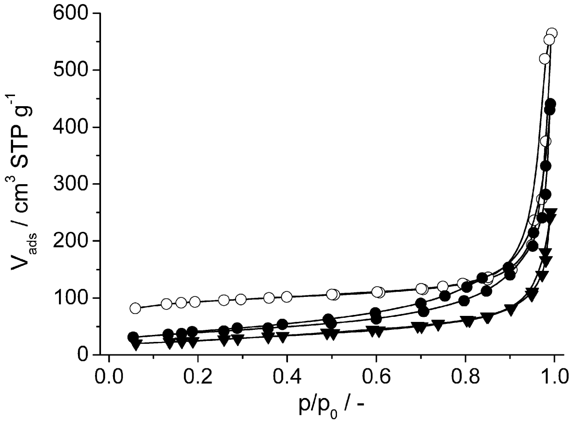

Fig. 3. Nitrogen isotherms at 77 K of (▼) carbon (CB), (○) precursor (LFA-BC-0), and (●) precursor–carbon composite (LFA-BC-25).

Table 1
Textural properties of selected samples

Sample	Treatment	V_{pore} ($\text{cm}^3\,\text{g}^{-1}$)	V_{micro}[a] ($\text{cm}^3\,\text{g}^{-1}$)	S_{meso}[a] ($\text{m}^2\,\text{g}^{-1}$)	S_{BET}[b] ($\text{m}^2\,\text{g}^{-1}$)
LFA-BC-0	Precursor	0.58	0.10	80	307
	Calcined at 973 K	0.70	0.08	112	266
	Calcined at 1473 K	0.06	0	11	11
LFA-BC-25	Precursor–carbon composite	0.43	0	137	137
	Calcined at 973 K	0.77	0.01	165	190
	Calcined at 1473 K	0.10	0	32	32
BC	Carbon	0.27	0	80	80

[a] *t*-plot method.
[b] BET method.

sample only exhibits the background pattern corresponding to the carbon (Fig. 1). In a similar manner, Schwickardi et al. [22] generally did not detect any crystalline phase upon impregnation of metal nitrates on activated carbon, which was attributed to the formation of small metal nitrate particles confined in the pore system of the template. The occurrence of XRD-invisible AACH crystallites, i.e. in the low nm-range, could indeed explain the absence of diffraction lines in LFA-BC-25. However, the formation of an amorphous phase distinct from AACH when the coprecipitation was conducted in the presence of carbon cannot be ruled out. In line with X-ray diffraction, transmission electron microscopy demonstrates the radically different morphology of the non-templated and templated precursors. In the composite (Fig. 2, bottom), the hexaaluminate precursor is deposited onto the carbon particles. The carbon black consists of spherical particles with an average size of 70 nm (Fig. 2, top). The size of the agglomerates increases substantially in the composite (around 100 nm), implying the coating of the carbon particles by the hexaaluminate precursor during the coprecipitation step.

The N_2 isotherm of the carbon black (Fig. 3, inverted triangles) is of type II according to IUPAC nomenclature [29], implying non-porous or macroporous properties. The BET surface area (80 $\text{m}^2\,\text{g}^{-1}$) results from textural porosity, i.e. surface roughness of the particles and interparticle voidage. The coating of the carbon particle by the precipitate induces mesoporous properties by partial filling of the interparticle space. The development of mesoporosity can be concluded from the uptake in the isotherm of LFA-BC-25 at intermediate relative pressures (Fig. 3, solid circles) and the textural parameters in Table 1. Interestingly, the composite has no microporosity, in contrast with LFA-BC-0, which is predominantly microporous. This implies that the morphology and texture of the precursor phase in the non-templated and templated samples presents marked differences, although it does not necessarily imply that different phases are obtained. Camblor et al. [30] previously demonstrated that zeolite nanocrystals present a distinct lower microporosity or even absence of microporosity as the crystal size decreases into the lower nm-range. This reasoning could apply to our system, i.e. the absence of microporosity in the templated sample being attributed to the small crystal size of the precursor species. In addition, the presence of small crystallites can also explain the higher mesopore surface area of 137 $\text{m}^2\,\text{g}^{-1}$ in the composite as compared to 80 $\text{m}^2\,\text{g}^{-1}$ in LFA-BC-0. The precursors were also characterized by He pycnometry. The skeleton density of the AACH precursor in LFA-BC-0 (2.53 $\text{cm}^3\,\text{g}^{-1}$) was slightly higher than that of carbon black (2.15 $\text{cm}^3\,\text{g}^{-1}$), and as expected the LFA-BC-25 composite had an intermediate value (2.34 $\text{cm}^3\,\text{g}^{-1}$).

3.2. Thermal activation

The thermogravimetric profile of LFA-BC-0 in air shows a one-step weight loss in the range 420–500 K (Fig. 4, top), which is assigned to the decomposition of the AACH phase [13,31]. The transition temperature was determined at 477 K from the derivative of the weight loss (Fig. 4, bottom). The total weight loss of the sample was slightly above 50%. The combustion of pure carbon black occurs at much higher temperature, starting at 1000 K and being completed at 1200 K (transition at 1125 K). The LFA-BC-25 composite shows a two-step decomposition pattern with a total weight loss of ca. 80%. The first weight loss occurs at 477 K, i.e. exactly the same temperature as in the non-templated sample. This suggests the occurrence of the same AACH phase in both precursors, i.e. the presence of carbon in the synthesis does not alter the chemical nature of the precipitate. On this basis, we put forward that the invisibility of AACH reflections in the XRD pattern of LFA-BC-25 in Fig. 1 and the absence of microporosity are consequences of the nanocrystalline nature of the AACH phase in the composite. The second weight loss in LFA-BC-25 (transition at 830 K) is associated with the combustion of carbon, although it occurs at ca. 300 K lower temperature than in pure carbon. The shift to lower temperature in the composite was also noticed by Schwickardi et al. [22] and is due to the catalyzed combustion of the template by the intermediate mixed metal oxide obtained upon decomposition of the precursor. The first and second steps of weight loss in LFA-BC-25 amount to ca. 30 and 50%, respectively. Accordingly, 37 wt% of this composite is oxide precursor and the remaining 63 wt% is carbon.

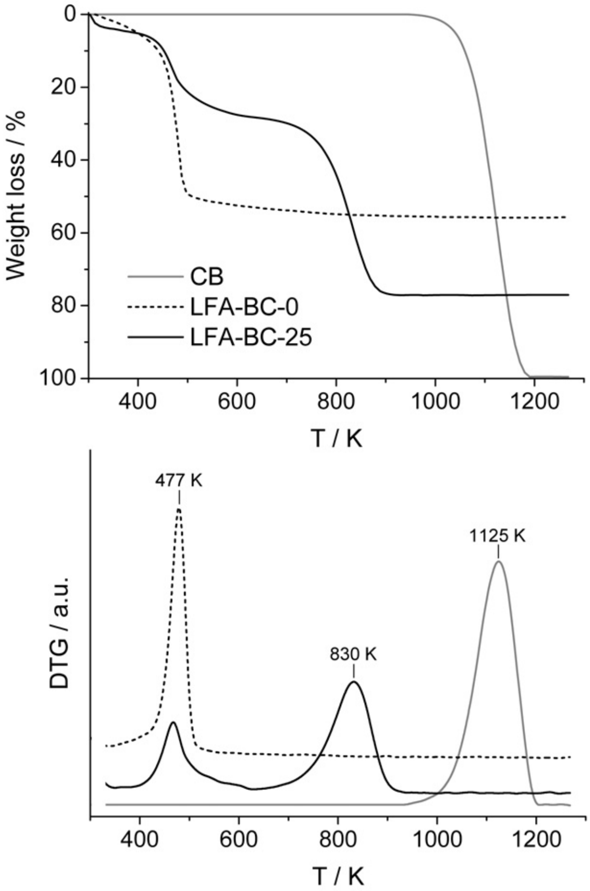

Fig. 4. Thermogravimetric profiles (top) and the resulting derivative curves (bottom) of carbon (CB), precursor (LFA-BC-0), and precursor–carbon composite (LFA-BC-25).

In situ X-ray diffraction during thermal activation of LFA-BC-0 and LFA-BC-25 in air was carried out to study the evolution of the precursors toward the hexaaluminate and to determine whether the presence of carbon in the composite has any effect on e.g. transition temperatures or occurrence of additional or intermediate crystalline phases during thermal activation. Fig. 5 shows the patterns of the samples at temperatures where relevant changes occurred. The characteristic reflections of AACH in LFA-BC-0 vanished at 473 K, leading to an amorphous oxide phase. This temperature is in excellent agreement with thermogravimetry. The XRD of the sample remains silent until 1373 K, where distinctive reflections of $LaFeAl_{11}O_{19}$ (JCPDS 36-1314) start to appear. The hexaaluminate pattern develops on increasing the temperature due to its progressive crystallization.

In correspondence with ex situ measurements in Fig. 1, the pattern of the LFA-BC-25 composite only displayed the broad reflections at $2\theta = 25^\circ$ and 43° belonging to carbon. The intensity of this reflection gradually decreases with increasing temperature and ultimately disappears at 873 K, in concordance with the occur-

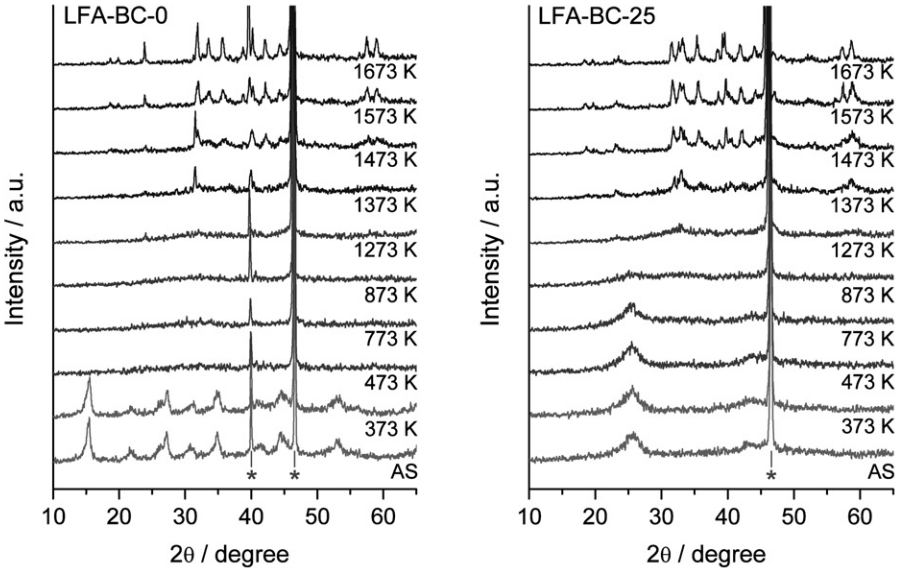

Fig. 5. In situ X-ray diffraction patterns at selected temperatures during thermal activation of LFA-BC-0 and LFA-BC-25 in air. The reflections marked by asterisk are due to the Pt_{90}–Rh_{10} heater strip.

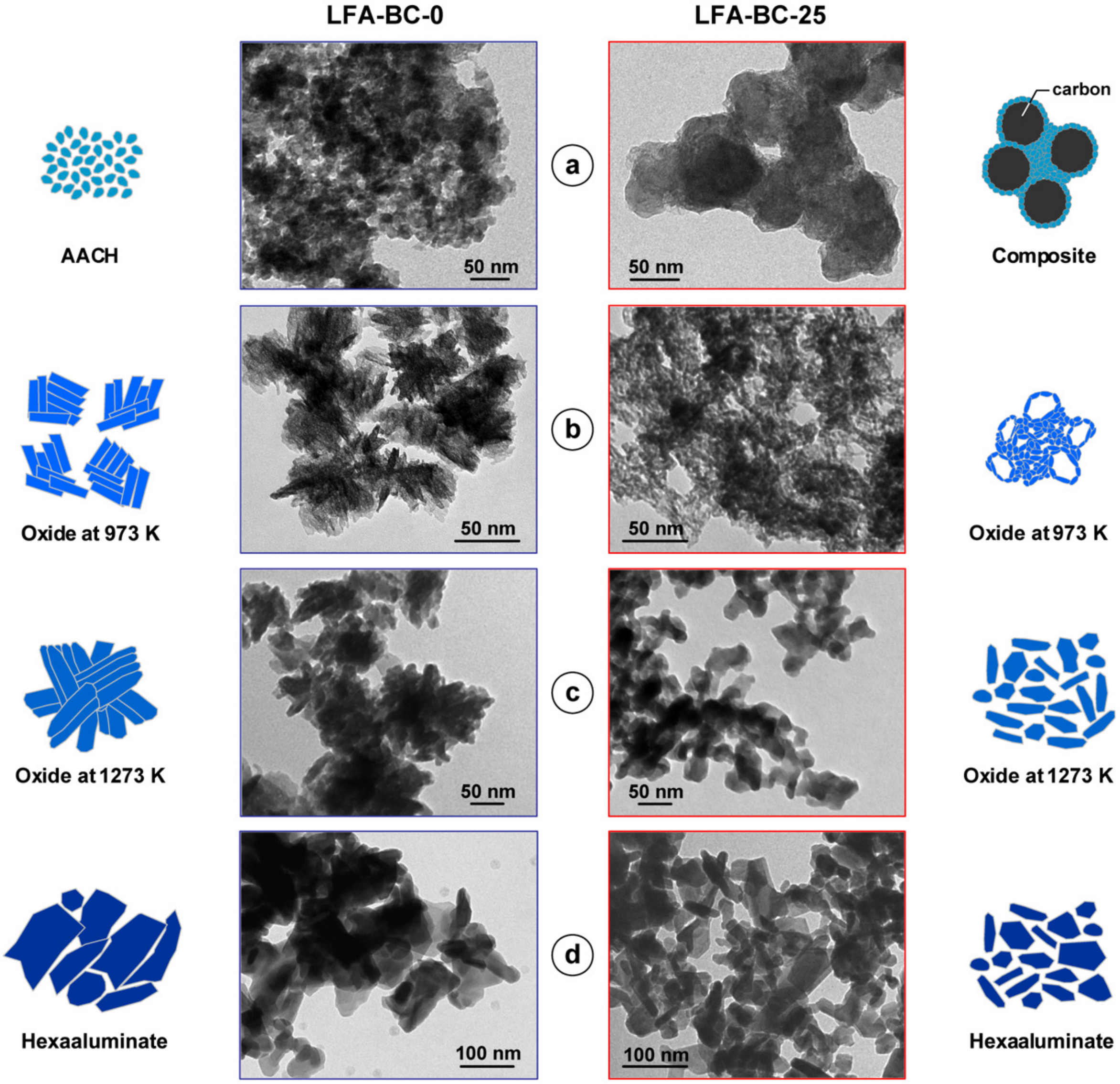

Fig. 6. Transmission electron micrographs and pictorial schemes of the samples at different stages during preparation of $LaFeAl_{11}O_{19}$ from LFA-BC-0 (non-templated) and LFA-BC-25 (carbon templated) precursors.

rence of the weight loss due to carbon combustion in Fig. 4. As in the non-templated sample, characteristic reflections of $LaFeAl_{11}O_{19}$ appear in the pattern at 1373 K, i.e. the incorporation of carbon did not noticeably affect to the temperature at which the hexaaluminate is formed. In both non-templated and templated oxides, $LaFeAl_{11}O_{19}$ was the only crystalline phase present.

Fig. 6 summarizes the morphological changes of the samples prepared by coprecipitation with and without carbon at different stages of the thermal treatment toward the hexaaluminate. Selected temperatures, based on TGA and in situ XRD analysis, were 973 K (at which carbon removal is completed), 1273 K (just before hexaaluminate formation), and 1473 K (at which well-crystallized hexaaluminate is attained). In the conventional method, i.e. without carbon, the spherical-like nanoparticles in the precipitate developed into platelets upon calcination at 973 K (Fig. 6b, left). The platelets extensively agglomerate on further heating, leading to anisotropic elongated hexaaluminate particles with a broad size distribution in the range 40–110 nm (Fig. 6d, left). The corresponding carbon-templated samples present remarkable morphological differences. The intermediate oxide at 973 K shows very small particles (5–10 nm) (Fig. 6b, right) in contrast with the larger platelets in the carbon-free synthesis. The LFA-BC-25 sample at 973 K clearly shows voids in the structure being the heritage of the carbon that was removed upon combustion. In fact, holes in the size range 20–30 nm can be visualized in the micrograph (also confirmed by N_2 adsorption, vide infra). Carbon removal in our templated sample does not result in hollow sphere architectures with an outer shell of the oxide as found in synthesis routes using ordered meso- and macroporous carbons [32,33]. The formation of hollow spheres is favored when the oxide shell surrounding the carbon particle is continuous and relatively thick (in the order of 100 nm [33]), since the strength of the shell is thereby increased. A relatively thin layer of oxide does not resist the pressure generated upon release of CO_2 and H_2O on carbon combustion, fragmenting it into smaller particles. In fact, the vigorous process of carbon removal, cracking the outer shell of the intermediate oxide, could be responsible for the attainment of small oxide particles and large void fraction.

Schwickardi et al. [22] proposed that the confinement of the metal nitrate in the pores of an activated carbon with well-developed micro- and mesoporosity ($S_{BET} = 1500\ m^2\,g^{-1}$), is most probably the origin of small oxide particles and hence high surface areas. This concept can be simplistically visualized as 'dispersing' the metal oxide precursor in the carbon pore network so that

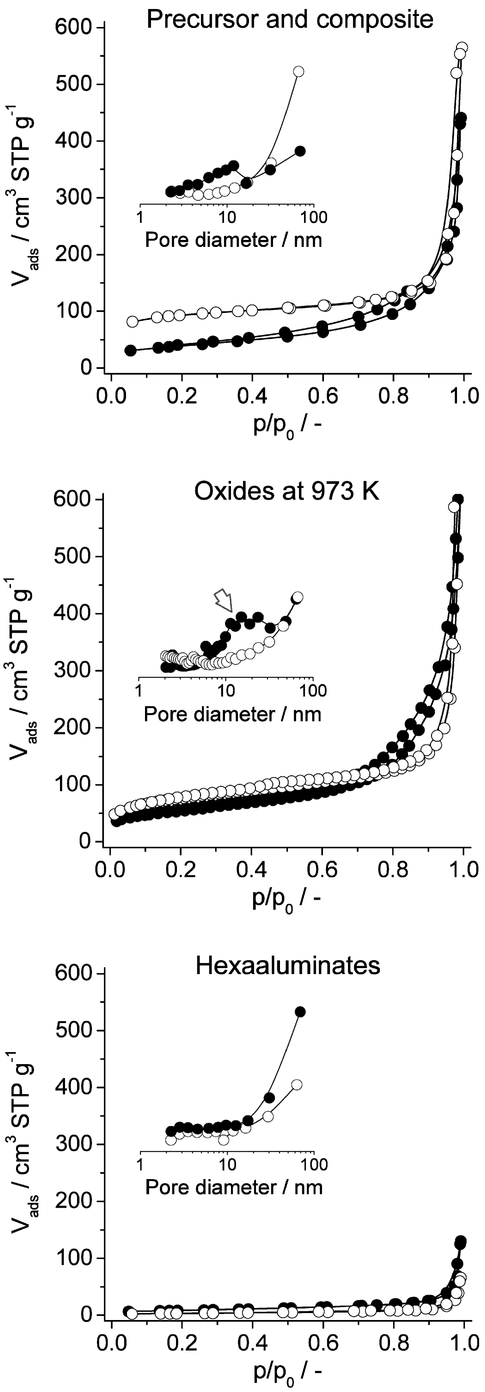

Fig. 7. Nitrogen isotherms at 77 K of (○) LFA-BC-0 and (●) LFA-BC-25 at different stages during preparation of $LaFeAl_{11}O_{19}$. Insets: adsorption BJH pore size distributions.

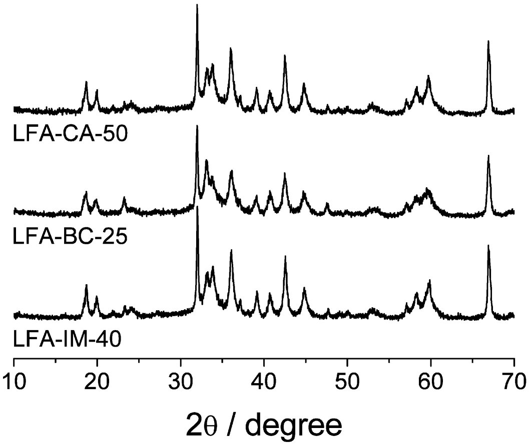

Fig. 8. Ex situ X-ray diffraction patterns of carbon-templated $LaFeAl_{11}O_{19}$ obtained by different synthesis routes. The reflections correspond to $LaFeAl_{11}O_{19}$, JCPDS 36-1314.

agglomeration is reduced. Since our carbon black is purely macroporous (Fig. 3 and Table 1), this mechanism can be discarded at an intraparticle level. However, we cannot rule out the confined space synthesis mechanism caused by the interparticle space, which also limits the growth of hexaaluminate precursor. As shown by TEM of the LFA-BC-25 composite (Fig. 2), the precipitate should be mostly deposited over the external surface of the carbon particles. Accordingly, we put forward that the confinement-based mechanism [22] is not uniquely responsible for small oxide particles by exotemplating approaches. The precipitation of small crystallites in our composite and particle breakage of oxide particles originated by the carbon combustion process are also important for attaining finely dispersed oxide particles.

The small particles in LFA-BC-25 treated at 973 K certainly grow on increasing the temperature for the attainment of the hexaaluminate phase at 1473 K, but the TEM micrographs in Fig. 6d clearly visualized much smaller particles in LFA-BC-25 as compared to LFA-BC-0. A priori, one could anticipate that the small particles of the intermediate oxide at 973 K would grow extensively up to 1473 K, ultimately resembling the hexaaluminate prepared in the absence of carbon. However, the positive effect of carbon toward smaller particles (higher external surface) occurs despite the 300 K difference between the elimination of carbon by combustion and the formation of the hexaaluminate. Consequently, the unique morphology of the intermediate oxide determines the morphology of the final oxide.

Fig. 7 and Table 1 show the evolution of the textural properties of the as-synthesized samples with and without template and the respective oxides calcined at 973 K and 1473 K. The differences in porosity between the precursor and composite samples were discussed in the previous section. Interestingly, a significantly higher BET surface area of 266 $m^2\,g^{-1}$ is obtained over the oxide at 973 K derived from the carbon-free method compared to the carbon-templating route (190 $m^2\,g^{-1}$). This is attributed to a pronounced contribution of microporosity (0.08 $cm^3\,g^{-1}$) to the total surface area of LFA-BC-0, which is substantially lower (0.01 $cm^3\,g^{-1}$) in LFA-BC-25. The latter sample evidences a higher mesopore surface area of 165 $m^2\,g^{-1}$, mostly obtained by 20–30 nm pores as evidenced in the BJH pore size distribution (inset). This is in good agreement with TEM investigations (Fig. 6b, right) and is the result of the templating effect. The hexaaluminate synthesized by the carbon templating route presents a three times higher surface area than the non-templated counterpart (32 vs 11 $m^2\,g^{-1}$) and a somewhat higher total pore volume, as revealed by the increased adsorbed volume at higher relative pressures in the N_2 isotherm. This result ultimately proves the positive effect of the carbon templating route in achieving higher surface areas over high-temperature catalysts such as hexaaluminates.

3.3. Hexaaluminates

Ex situ XRD patterns of representative samples obtained by calcination of the differently prepared precursors are shown in Fig. 8. $LaFeAl_{11}O_{19}$ was the only crystalline phase observed, regardless the synthesis route and the carbon content in the precursor. The chemical composition of several non-templated and templated

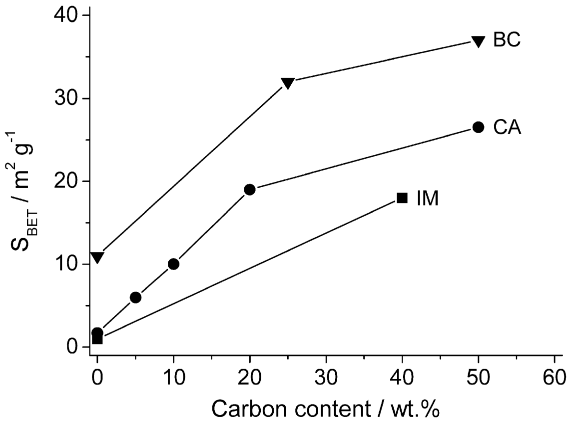

Fig. 9. BET surface area of $LaFeAl_{11}O_{19}$ vs the nominal carbon content for different preparation methods.

hexaaluminates was determined by ICP–OES. The molar metal ratios in the solids were in all cases very close to the nominal values (La:Fe:Al = 1:1:11), indicating that the preparations were carried out effectively. The positive effect of carbon templating on the specific surface area of the resulting hexaaluminate has been observed for all the preparation methods. The BET surface area gradually increases with increasing the nominal carbon content in the composite (Fig. 9). The surface area of the non-templated hexaaluminate prepared by coprecipitation is higher than the counterparts prepared by the other two methods. It is then clear that the synthesis route of the precursor is also crucial to maximize the surface area by arriving at smaller hexaaluminate particles. The surface area of the non-templated samples prepared by impregnation and complexation (1–2 $m^2\,g^{-1}$) is enhanced by a factor of 4–25 (depending on the synthesis route) when carbon was incorporated in the synthesis. The highest surface area was attained in the hexaaluminate prepared by coprecipitation using a nominal carbon content of 50 wt% (ca. 40 $m^2\,g^{-1}$). Application of reverse-microemulsion routes generally leads to hexaaluminates with higher surface areas (40–160 $m^2\,g^{-1}$) [15,16,34]. However, the template route using carbon is regarded as highly attractive when balancing the significant increase in surface area of the oxide and the utilization of scalable methods (coprecipitation, impregnation, complexation) for large-scale synthesis of this type of materials.

Prior to demonstrating the benefits of the carbon-templated hexaaluminates in catalytic applications, it is important to evaluate the potential impact of carbon on the nature of the species in the oxide as compared to the hexaaluminate prepared in the absence of template. In the prospects of the work by Schwickardi et al. [22], it is hypothesized that for oxides with easily reduced metal ions, intermediate reactions might take place during carbon removal that could lead to low-valence crystalline phases. We have conducted temperature-programmed reduction with hydrogen and X-ray photoelectron spectroscopy in order to comparatively investigate the nature of iron in the non-templated and templated $LaFeAl_{11}O_{19}$ hexaaluminates. The H_2-TPR profiles in Fig. 10 show different regions of hydrogen consumption. The peaks centered at 700 and 900 K can be attributed to the formation of ferrous ions and the consumption above 1100 K is assigned to the reduction into metallic iron. Importantly, the results show the practically identical profiles with respect to peak position and amount of hydrogen consumed in the non-templated and templated hexaaluminates, indicating that the nature and amount of redox-active iron species in the oxide are not significantly affected by the incorporation of carbon in the synthesis. However, the H_2-TPR analyses are not meant to quantitatively determine the oxidation state of iron in the samples, since the assignment of the various overlapped hydrogen consumption peaks is not definitive.

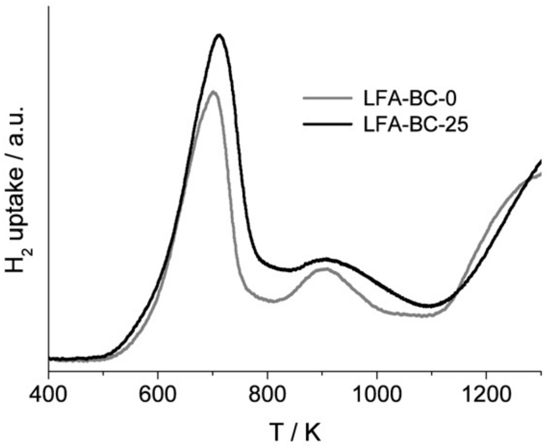

Fig. 10. H_2-TPR profiles of $LaFeAl_{11}O_{19}$ prepared by coprecipitation in the absence or presence of carbon.

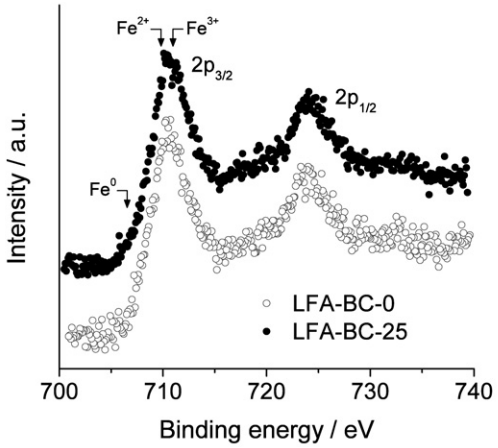

Fig. 11. Fe 2p core-level spectra of $LaFeAl_{11}O_{19}$ prepared by coprecipitation in the absence or presence of carbon.

The Fe 2p core level XPS spectra of LFA-BC-0 and LFA-BC-25 (Fig. 11) is practically identical, further supporting that the incorporation of carbon in the synthesis does not alter the nature of iron in the final catalysts. The core level XPS spectra of other elements in the hexaaluminate were very similar too. The atomic metal ratio determined by XPS was La/Fe/Al = 1.3/0.9/11 in LFA-BC-0 and 1.2/0.8/11 in LFA-BC-25, indicating a certain enrichment of lanthanum at the hexaaluminate surface with respect to bulk analyses (La/Fe/Al = 1/1/11). The position of the broad peak centered at 710.5 eV in Fig. 11 is intermediate between those typically reported for Fe(II) (709.9 eV) and Fe(III) (710.8 eV) [35]. Based on this, the presence of both ferric and ferrous ions in the hexaaluminates can be put forward. Metallic iron, with a characteristic binding energy of 706.5 eV [35], can be safely excluded in the samples. The presence of both Fe^{2+} and Fe^{3+} in different lattice positions of a $LaFeAl_{11}O_{19}$ single crystal (annealed in air at 1773 K) was convincingly shown by Lejus et al. [36,37] using XRD, EPR, UV–vis DR spectroscopy, and Mössbauer spectroscopy. In particular, Fe^{2+} (ca. 32% of the iron in the sample) was concluded to be preferentially located in tetrahedral sites of the lattice, while Fe^{3+} (the remaining 67%) appears in tetrahedral as well as bipyramidal sites. The nature of iron in the more widely studied $BaFeAl_{11}O_{19}$ (β-Al_2O_3 structure) is substantially different compared to $LaFeAl_{11}O_{19}$ (magnetoplumbite structure). In the for-

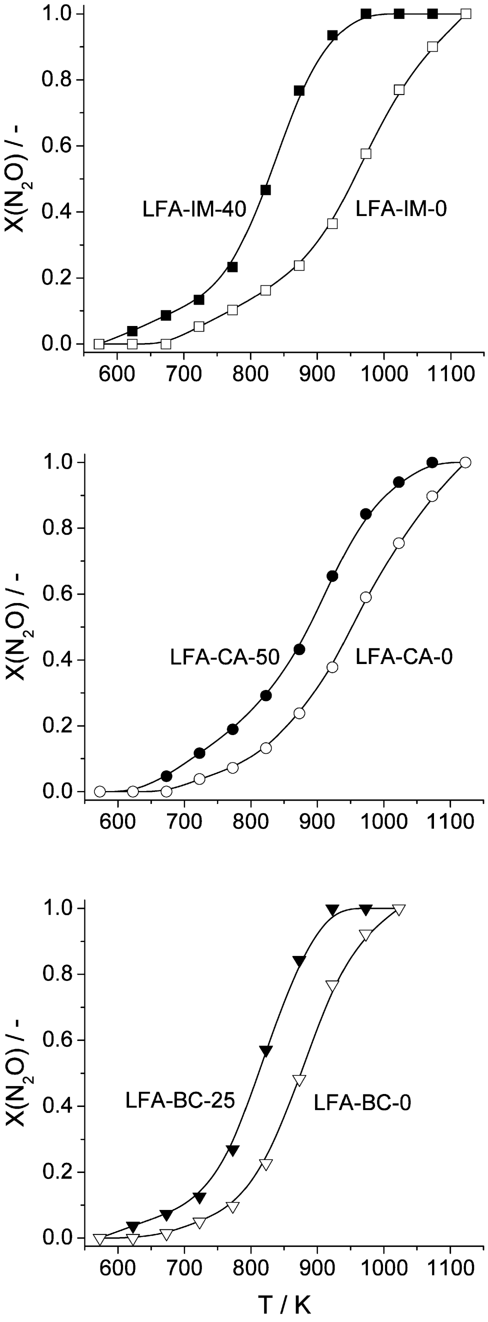

Fig. 12. N_2O conversion vs temperature over differently synthesized $LaFeAl_{11}O_{19}$ in the absence or presence of carbon. Conditions: 1.5 mbar N_2O in He, WHSV = 60,000 $ml\,g^{-1}\,h^{-1}$, $P = 1$ bar.

mer, iron is exclusively trivalent and occupies octahedral coordination [5,7,38].

3.4. Catalytic activity

Our previous work [11] demonstrated the excellent performance of non-templated metal-substituted hexaaluminates under simulated process conditions at the outlet of the Pt–Rh gauzes in ammonia burners, i.e. in a mixture containing N_2O, NO, O_2, and H_2O. This manuscript aims at generally demonstrating the improved activity of carbon-templated hexaaluminates with respect to equivalent syntheses in the absence of carbon. For this purpose, a model mixture with $N_2O + He$ was used in the first place. Fig. 12 shows the N_2O conversion vs temperature profiles over selected $LaFeAl_{11}O_{19}$ hexaaluminates. Both the preparation method and the incorporation of carbon during the synthesis of the hexaaluminate impact on the catalytic performance. In the absence of carbon, the sample prepared by coprecipitation (BC) displays higher activity than the samples prepared by complexation (CA) and impregnation (IM). The T_{50} (temperature for 50% N_2O conversion) is 875 K over LFA-BC-0, shifting to 950 K and 975 K over LFA-CA-0 and LFA-IM-0, respectively. The templating effect of carbon proves beneficial for the catalytic performance, independent on the synthesis method applied. Accordingly, the light-off is shifted 50–100 K to lower temperature compared to the non-templated samples. As expected, the largest improvement was observed in the sample prepared by impregnation due to the very low surface area of the non-templated hexaaluminate (1 $m^2\,g^{-1}$, Fig. 9). As elaborated in the previous section, H_2-TPR and XPS characterizations demonstrated that the nature of the iron species in the hexaaluminates prepared was not altered by the incorporation of carbon in the synthesis. Accordingly, the positive effect on the catalytic activity can be exclusively assigned to the enhanced surface area resulting from the stabilization of fine particles induced by the template.

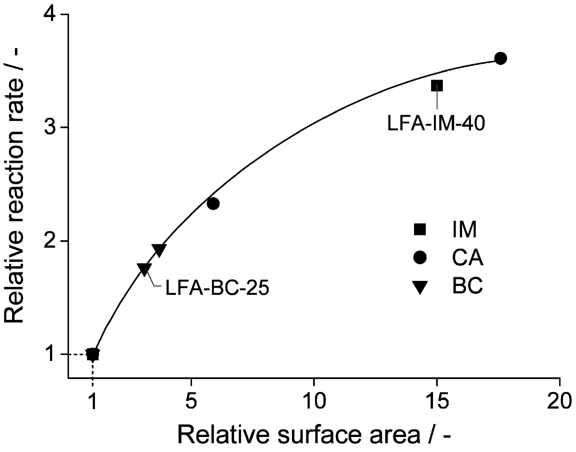

Fig. 13. Rate of N_2O decomposition vs BET surface area of $LaFeAl_{11}O_{19}$. The values of reaction rate and specific surface area are relative to those of the non-templated hexaaluminates for each preparation method. Conditions: 1.5 mbar N_2O in He, $T = 850$ K, WHSV = 60,000 $ml\,g^{-1}\,h^{-1}$, $P = 1$ bar.

Fig. 13 plots the relative reaction rate for N_2O decomposition vs the relative surface area for the catalysts. The values of reaction rate and surface area of the carbon-templated hexaaluminates were normalized with respect to the non-templated counterparts for each preparation method. The reaction rate was determined at 850 K; at this temperature, the degree of N_2O conversion over the catalysts ranges from 20 to 80%. The dependence is quasi-linear, indicating that the specific surface area is a prime performance indicator of the catalyst. For example, carbon incorporation in LFA-IM-40 leads to an increased surface area of 15 times with respect to the non-templated LFA-IM-0 counterpart and the reaction rate is 3.5 times higher. In LFA-BC-25, where S_{BET} was 3 times higher than in LFA-BC-0, the reaction rate for N_2O decomposition is doubled. The templated hexaaluminates exhibit smaller particle size, i.e. higher surface-to-volume ratios, than the non-templated ones and therefore eventual external diffusion limitations are alleviated. The flattened dependence in Fig. 13 upon increasing the surface area can be explained as follows. Below a certain particle size, external diffusion limitations become less important and the chemical regime dominates. In consequence, the surface area of the catalyst has a less marked influence on the reaction rate. Certainly, internal diffusion cannot explain this behavior since hexaaluminates are practically non-porous, i.e. the total surface area

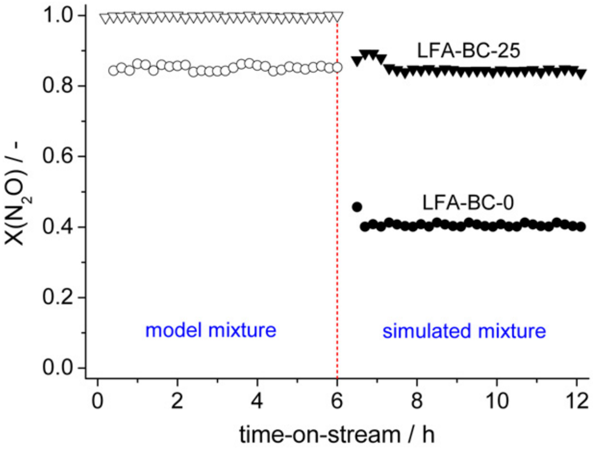

Fig. 14. N_2O conversion vs time-on-stream over (○, ●) LFA-BC-0 and (▽, ▼) LFA-BC-25 in a model mixture (open symbols) containing 1.5 mbar N_2O in He and in a simulated mixture (solid symbols) containing 1.5 mbar N_2O, 10 mbar NO, 100 mbar O_2, 100 mbar H_2O in He. Conditions: $T = 923$ K, WHSV = 60,000 ml g^{-1} h^{-1}, $P = 1$ bar.

derives from the external surface (particle size effect) and surface roughness.

It can be anticipated that the beneficial effect of carbon templating in a model $N_2O + He$ feed will remain in mixtures simulating more closely process conditions. To demonstrate that, we conducted isothermal tests over LFA-BC-0 and LFA-BC-25 in a feed containing N_2O, NO, O_2, and H_2O. This mimics the outlet gas of the Pt–Rh gauzes in ammonia burners, where N_2O decomposition at high temperature (process-gas option) is practiced [11,41]. As shown in Fig. 14, the N_2O conversion was significantly higher over the templated hexaaluminate in model and in simulated feeds. In addition, the stability of the catalysts was remarkable in the 6 h testing period. It is essential for practical implementation that the improved porous properties of the hexaaluminates due to carbon templating are preserved during process operation. We confirmed that the relatively high surface area of LFA-BC-25 was fully retained after 6 h on stream at 923 K. This was foreseen, since the calcination temperature to form the hexaaluminate (1473 K) is several hundreds of degrees higher than the temperature at the outlet of the noble metal gauzes in the ammonia burner.

Finally, it should be stressed that comparing the de-N_2O performance of metal-substituted hexaaluminates with low-temperature catalysts such as calcined hydrotalcites and zeolites loaded with transition and noble metals [39–41] is not feasible since both systems need to fulfill markedly different requirements and are thus installed in different locations of the process [24]. In the case of nitric acid production, the major source of N_2O in the chemical industry, low-temperature catalysts (displaying activity <773 K) are applied in the tail-gas train. Contrarily, the intrinsically less active hexaaluminates and other mixed oxide catalysts such as perovskites are installed right after the noble metal gauzes in the ammonia burner. The latter systems must satisfy the number one condition of chemical stability coupled to high catalytic activity for implementation in the harsh environment of the ammonia burner (high temperature and wet oxidizing conditions). Low-temperature catalysts can be discarded under these conditions due to lack of chemical and/or thermal stability.

4. Conclusions

Incorporation of a commercial non-ordered macroporous carbon in the synthesis of metal-substituted hexaaluminates ($LaFeAl_{11}O_{19}$) leads to increased surface areas and improved catalytic performance in N_2O decomposition as compared to the non-templated counterparts. The BET surface area of the oxides is enhanced by a factor of 4–25, depending on the synthesis route and the amount of carbon incorporated. The templating action of carbon leads to finely dispersed hexaaluminate particles, despite the large temperature difference between the combustion of carbon (973 K) and the hexaaluminate formation (1473 K). Analyses of intermediate phases on transformation of the as-synthesized composites into the final hexaaluminates revealed fundamental understanding of the template action. The morphology of the oxide obtained upon carbon removal determines the final properties of the hexaaluminate particles. The growth of small crystallites at the carbon surface in the composite and the vigorous combustion of the template are key aspects in the attainment of small particles through fragmentation of the oxide layer deposited on the template. The confined space synthesis mechanism also contributes. However, it may play a less significant role attending to the purely macroporous nature of the carbon used in this study. The highest surface area was attained in the hexaaluminate prepared by coprecipitation using 50 wt% of carbon (ca. 40 m^2 g^{-1}). This value is lower than reported hexaaluminates using reverse micro-emulsion methods. Advantageously, the templating route is more amenable to practical implementation due its versatility, low cost, simplicity, and scalability. The carbon-templated $LaFeAl_{11}O_{19}$ is more active for N_2O decomposition than the non-templated counterpart and displays stable conversion in simulated mixtures (containing N_2O, NO, O_2, and H_2O). Our tests demonstrate a quasi-linear correlation between the reaction rate and the specific surface area of the samples. The improved catalytic performance is related to the increased specific surface area of the hexaaluminate, as the nature of iron in the oxide in non-templated and templated oxides was not affected by the incorporation of carbon in the synthesis. Consequently, the carbon-assisted templating route enables the preparation of more efficient high-temperature catalysts, combining reduced light-off temperature with high stability.

Acknowledgments

This research was sponsored by the Spanish MEC (project CTQ2006-01562/PPQ and Consolider-Ingenio 2010, grant CSD2006-003) and the ICIQ Foundation. N.M. van der Pers at the Department of Materials Science and Engineering of TUDelft is acknowledged for the in situ X-ray analyses and M.S. Yalfani for experimental input.

References

[1] M. Machida, K. Eguchi, H. Arai, J. Catal. 103 (1987) 385.
[2] M. Machida, K. Eguchi, H. Arai, J. Catal. 120 (1989) 377.
[3] M.F.M. Zwinckels, S.G. Järås, P.G. Menon, T.A. Griffin, Catal. Rev. Sci. Eng. 35 (1993) 319.
[4] G. Groppi, M. Bellotto, C. Cristiani, P. Forzatti, P.L. Villa, Appl. Catal. A 104 (1993) 101.
[5] L. Lietti, C. Cristiani, G. Groppi, P. Forzatti, Catal. Today 59 (2000) 191.
[6] G. Groppi, C. Cristiani, P. Forzatti, Appl. Catal. B 35 (2001) 137.
[7] P. Artizzu-Duart, J.M. Millet, N. Guilhaume, E. Garbowski, M. Primet, Catal. Today 59 (2000) 163.
[8] T.V. Chouldhary, S. Banerjee, V.R. Choudhary, Appl. Catal. A 234 (2002) 1.
[9] R. Kikuchi, Y. Iwasa, T. Takeguchi, K. Eguchi, Appl. Catal. A 281 (2005) 61.
[10] Z. Xu, M. Zhen, Y. Bi, K. Zhen, Appl. Catal. A 198 (2000) 267.
[11] J. Pérez-Ramírez, M. Santiago, Chem. Commun. (2007) 619.
[12] M. Machida, K. Eguchi, H. Arai, J. Am. Ceram. Soc. 71 (1988) 1142.
[13] M.S. Yalfani, M. Santiago, J. Pérez-Ramírez, J. Mater. Chem. 17 (2007) 1222.
[14] P. Forzatti, G. Groppi, Catal. Today 54 (1999) 165.
[15] A.J. Zarur, J.Y. Ying, Nature 403 (2000) 65.
[16] F. Teng, Z. Xu, G. Xiong, Y. Xu, Z. Xu, L. Lin, Green Chem. 7 (2005) 493.
[17] F. Schüth, Angew. Chem. Int. Ed. 42 (2003) 3604, and references therein.
[18] K.J.C. van Bommel, A. Friggeri, S. Shinkai, Angew. Chem. Int. Ed. 42 (2003) 980.
[19] X.S. Zhao, F. Su, Q. Yan, W. Guo, X.Y. Bao, L. Lv, Z. Zhou, J. Mater. Chem. 16 (2006) 637.

[20] C. Madsen, C.J.H. Jacobsen, Chem. Commun. (1999) 673.
[21] M. Kustova, K. Egeblad, K. Zhu, C.H. Christensen, Chem. Mater. 19 (2007) 2915.
[22] M. Schwickardi, T. Johann, W. Schmidt, F. Schüth, Chem. Mater. 14 (2002) 3913.
[23] J. Blanco, A.L. Petre, M. Yates, M.P. Martin, S. Suarez, J.A. Martin, Adv. Mater. 18 (2006) 1162.
[24] J. Pérez-Ramírez, F. Kapteijn, K. Schöffel, J.A. Moulijn, Appl. Catal. B 44 (2003) 117.
[25] J. Pérez-Ramírez, B. Vigeland, Angew. Chem. Int. Ed. 44 (2005) 1112.
[26] S. Brunauer, P.H. Emmett, E.J. Teller, J. Am. Chem. Soc. 60 (1938) 309.
[27] B.C. Lippens, J.H. de Boer, J. Catal. 4 (1965) 319.
[28] E.P. Barret, L.G. Joyner, P.H. Hallenda, J. Am. Chem. Soc. 73 (1951) 373.
[29] K.S.W. Sing, D.H. Everett, R.A.W. Haul, L. Moscou, R.A. Pierotti, J. Rouquerol, T. Siemieniewska, Pure Appl. Chem. 57 (1985) 603.
[30] M.A. Camblor, A. Corma, S. Valencia, Microporous Mesoporous Mater. 25 (1998) 59.
[31] G. Stoica, J. Pérez-Ramírez, Chem. Mater. 19 (2007) 4783.
[32] L. Zhibin, L. Jianmin, K. Yanxiong, Y. Zhang, H. Zhang, L. Fanqing, X. Jinyun, J. Mater. Chem. 11 (2001) 2930.
[33] X. Yongde, R. Mokaya, J. Mater. Chem. 15 (2005) 3126.
[34] Z. You, K. Inazu, K. Aika, T. Baba, J. Catal. 251 (2007) 321.
[35] D.D. Hawn, B.M. DeKoven, Surf. Interface Anal. 10 (1987) 63.
[36] F. Laville, A.M. Lejus, J. Cryst. Growth 63 (1983) 426.
[37] E. Tronc, F. Laville, M. Gasperin, A.M. Lejus, D. Vivien, J. Solid State Chem. 81 (1989) 192.
[38] D. Naoufal, J.-M. Millet, E. Garbowski, Y. Brullé, M. Primet, Catal. Lett. 54 (1998) 141.
[39] Y. Li, J.N. Armor, Appl. Catal. B 1 (1992) L21.
[40] F. Kapteijn, J. Rodríguez-Mirasol, J.A. Moulijn, Appl. Catal. B 9 (1996) 25.
[41] J. Pérez-Ramírez, J. Overejinder, F. Kapteijn, J.A. Moulijn, Appl. Catal. B 23 (1999) 59.